Journal of Geoscience and Environment Protection, 2023, 11, 159-173
https://www.scirp.org/journal/gep
ISSN Online: 2327-4344
ISSN Print: 2327-4336

Seasonal Difference of the Spatio-Temporal Variation of Precipitable Water Vapor in China

Qixu Li[1,2], Qianqian Song[1], Zhitong Qian[1*], Ying Huang[3]

[1]Key Laboratory of Meteorological Disaster, Ministry of Education (KLME), Joint International Research Laboratory of Climate and Environment Change (ILCEC), Collaborative Innovation Center on Forecast and Evaluation of Meteorological Disasters (CIC-FEMD), Nanjing University of Information Science and Technology, Nanjing, China
[2]Meteorological Observatory of Tibet Autonomous Region, Lhasa, China
[3]Ningxia Climate Center, Yinchuan, China
Email: *qzt1041666347@163.com

How to cite this paper: Li, Q. X., Song, Q. Q., Qian, Z. T., & Huang, Y. (2023). Seasonal Difference of the Spatio-Temporal Variation of Precipitable Water Vapor in China. *Journal of Geoscience and Environment Protection, 11,* 159-173.
https://doi.org/10.4236/gep.2023.115010

Received: April 13, 2023
Accepted: May 27, 2023
Published: May 30, 2023

Abstract

This study analyzes the spatial and temporal distribution characteristics of seasonal precipitable water vapor (PWV) in China between 1979 and 2008. To achieve this, the observed temperature dew point difference and atmospheric pressure at various altitudes of 102 radiosonde stations were utilized. The analysis involved calculating and examining the PWV variations across the different seasons in the study period. The results are illustrated as follows: 1) The annual mean and seasonal mean PWV over China is characterized by decreasing from southeast to northwest. The PWV has obvious seasonal features. It is the least in winter, which is mainly affected by latitude and altitude, and the most in summer, which is mainly affected by the monsoon. It is the medium in spring and autumn, with more in autumn than in spring. 2) The spatial distribution pattern of four seasonal PWV is approximately opposite to its variation coefficient distribution pattern, that is, the monsoon (non-monsoon) areas with more (less) PWV have a smaller (larger) variation amplitude. 3) The distribution pattern of four seasonal PWV shows a consistent distribution pattern in the whole region and the winter characteristics are the most significant. The abnormal variation of PWV shows consistent interdecadal oscillation, and it exhibits an obvious phase transition around 2002 when the PWV has an increasing shift in winter, spring, and summer, while it is more complicated in autumn.

Keywords

Precipitable Water Vapor, Distribution Characteristics, Four Seasons

1. Introduction

Water vapor plays a pronounced role in climate change and hydrological processes (Chahine, 1992; Held & Soden, 2000). It is one of the most important greenhouse gases, which can account for two-thirds of the natural greenhouse effect and lead to further global warming through radiation effects (Kiehl & Trenberth, 1997; Wagner et al., 2006). In addition, it is an active and changeable component in the atmosphere, which has a major influence on the global water cycle and energy balance (Fontaine et al., 2003; Trenberth et al., 2007). The precipitable water vapor (PWV), the amount of vertically integrated water vapor, mainly reflects the richness of water vapor content in the atmosphere, which has unique spatial and temporal distribution of four seasonal PWV over China due to its complex topography and the influence of the East Asian summer monsoon. Accordingly, it is of great scientific significance to study the PWV for a better understanding of the water vapor feedback on global warming, reasonably developing water resources in the atmosphere, and predicting climate changes in the future (Held & Soden, 2000; Trenberth et al., 2005, 2007).

In recent years, many studies have been performed to detect the changes of PWV in China using a variety of reanalysis datasets (Shi & Sun, 2008; Liao et al., 2013; Ma et al., 2015; Huang et al., 2018a), which enrich the understanding of the temporal and spatial distribution of PWV. They mainly focus on the calculation and analysis of the whole region or a specific region of China. It is worth noting that reanalysis data includes errors brought by the change of observing system and introduced by assimilation schemes and numerical models. Therefore, the reanalysis data may not be reliable for some regions where the observation data are limited or absent for data assimilation (Oikonomou & O'Neill, 2006). Consequently, the errors may lead to the spurious long-term climate change of reanalysis water vapor (Zhao et al., 2010; Xie et al., 2011). Meanwhile, some scholars have pointed out that the applicability of reanalysis water vapor in different altitudes and seasons over China remains a vast distinction by comparing the specific humidity in reanalysis datasets and radiosonde dataset (Jia et al., 2014). In addition, some previous studies have revealed the climatic distribution characteristics of PWV in China using radiosonde dataset, mainly before the 1990s. Given high accuracy and vertical resolution of radiosonde water vapor, it is often used as the reference data in evaluating the performance of other water vapor measuring techniques (Brettle & Galvin, 2003; Liu et al., 2013a). It has been concluded that the distributions of PWV vary substantially in both space and time due to the influence of geographical latitude, altitude and monsoon. It is further confirmed that the PWV decreases from southeast to northwest and has significant seasonal variations (Zhai & Eskridge, 1997). However, there are some problems in these studies, such as the earlier data period of 1960-1969 (Zou & Liu, 1981; Lu & Gao, 1984), the shorter time series of 1957-1959 and the fewer stations (70 stations) (Zheng & Yang, 1962). At the same time, the radiosonde dataset has also been used to analyze the climatic distribution characteristics of PWV over the Tibetan Plateau (Zhou et al., 2011), North China

(Wang et al., 2017), Sichuan and Chongqing (Guo & Li, 2009), Ili River Basin (Yang et al., 2013), Northwest China (Huang et al., 2018b) and other regional areas. All these studies have provided a crucial reference for understanding the temporal and spatial distribution characteristics of PWV in China.

In summary, there are obvious regional differences and seasonal differences in the temporal and spatial distribution of PWV. In recent years, the research on PWV in China mostly focuses on a specific region of China, in the absence of the analysis of the whole region of China. Moreover, the research on the whole region of China is mainly based on reanalysis data, lacking analysis of observational data. In this paper, we implement the observational data of 102 radiosonde stations from 1979 to 2014 to investigate the distribution features of four seasonal PWV in China.

This paper is organized as follows. Section 2 describes the data and methods used in this study. In Section 3, the spatial distributions of annual, seasonal averaged PWV over Chinese mainland are examined. Moreover, the amplitude of variation of PWV is presented by calculating the coefficient of variation (the ratio of standard deviation to average). In Section 4, the empirical orthogonal function (EOF) decomposition (Wei, 2007) is used to reveal the spatial distribution and temporal variation of PWV in China. The conclusion and discussion are provided in Section 5.

2. Data and Method

2.1. Radiosonde Data

In this paper, the radiosonde data of 102 stations from 1979 to 2014 provided by the National Meteorological Information Center of the China Meteorological Administration are used. Radiosonde balloons are launched twice daily, at 0000 UTC and 1200 UTC (local time + 8 h). The meteorological parameters include temperature, temperature dew point difference and atmospheric pressure at different altitudes. **Figure 1** shows the spatial distribution of radiosonde stations.

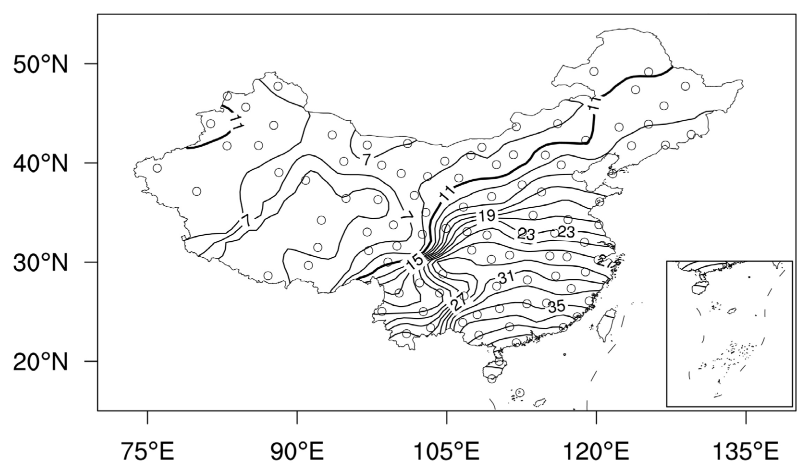

Figure 1. Annual mean PWV over Chinese mainland (unit: mm); the circles represent the spatial distribution of 102 radiosonde stations in China.

There are 62 radiosonde stations in eastern China (Referring to the area in the east of 105˚E, similarly hereinafter), accounting for more than 60% of total stations. There are few stations in the western part of the Tibetan Plateau. Additionally, the spring refers to March to May, the summer refers to June to August, the autumn refers to September to November, and the winter refers to December to February of the next year in this paper.

2.2. PWV Retrieval

Firstly, water vapor pressure (e) of each standard isobaric surface is determined by the dew point temperature (T_d) (The difference between the temperature and temperature dew point difference provided by the radiosonde data) as follows (Zhu et al., 2000):

$$e = 0.611 \times \exp\left(\frac{a \times T_d}{273.16 + T_d - b}\right) \tag{1}$$

where a and b are constants, and when the water surface is saturated, a = 17.26 and b = 35.86, respectively.

The specific humidity (q) is further obtained from the water vapor pressure as follows (Zhu et al., 2000):

$$q = 0.62197 \times \frac{e}{p - 0.378 \times e} \tag{2}$$

where p is the atmospheric pressure of each standard isobaric surface.

Finally, the PWV (mm) can be calculated from the vertically integrated water vapor column using the following equation (Zhou et al., 2011):

$$PWV = \frac{1}{g}\int_{P_t}^{P_s} q\mathrm{d}p \tag{3}$$

where g is gravitational acceleration, q is specific humidity, P_s is surface pressure, P_t is atmospheric pressure at the upper boundary of the integral, which is taken as 200 hPa in this paper due to little water vapor above it.

3. Climatological Characteristics of PWV

3.1. Spatial Distribution of Annual and Seasonal Mean PWV over Chinese Mainland

The radiosonde data have been used to calculate and analyze the spatial distribution of PWV in this study. **Figure 1** shows the spatial distribution of annual mean PWV over Chinese mainland from 1979 to 2014. The distribution of PWV in China showed clear geographical differences. Due to the influence of latitude, altitude, monsoon and other factors, the spatial distribution of PWV in China is generally characterized by low-latitude regions greater than high-latitude regions, plain regions greater than plateau regions, coastal regions greater than inland regions, and decreasing from southeast China to northwest China, which is basically consistent with the spatial distribution obtained by the NCEP/NCAR and ECMWF reanalysis (Dai & Yang, 2009; Liu et al., 2013a). The PWV contours in China roughly distribute along the parallel and vary along the latitude. Meanwhile, it can be seen that there is no intersection angle between the PWV contours and the parallel in southeast China but an intersection angle in other areas. Furthermore, the increasing PWV contours are associated with decreasing altitudes. The high PWV values prevail in South China with lower altitude ranging from 40 to 44 mm, while the low PWV values prevail over the Tibetan Plateau with the highest altitude, with PWV of lower than 5 mm. Therefore, the topography plays a crucial role in influencing the distribution of PWV: on the one hand, the orographic lift reduces the thickness of low-level air column with ample moisture resulting in less PWV in the total column; on the other hand, the barrier effect of topography blocks the water vapor input resulting in less PWV over the Tibetan Plateau (Zou & Liu, 1981; Liu et al., 2013b). It can be seen that the PWV contours are dense and have a large gradient in southwest China, which is also related to the large topography. The 11 mm PWV contour in **Figure 1** distributes along the Xiaoxing'an Mountain-Yinshan-Helan Mountain-Hengduan Mountain, which roughly corresponds to the separatrix between monsoon and non-monsoon areas over Chinese mainland and coincides with the demarcation line of population density, namely Heihe-Tengchong Line. Taking the 11 mm PWV contour as the boundary, the PWV in southeast China (monsoon areas) is about four times more than that in northwest China (non-monsoon areas), which indicates that the East Asian monsoon has a great influence on the spatial distribution of PWV in China.

Figure 2 further presents the spatial distribution of the 30-year averaged PWV for winter, spring, summer, and autumn. Overall, the seasonal mean PWV is characterized by decreasing from South China Coastal to northwest interior over Chinese mainland and shows pronounced seasonal variations. Its values are lowest in winter, followed by spring and autumn, and are highest in summer, which are consistent with previous studies (Zhao et al., 2012; Wong et al., 2015; Wang et al., 2017). Winter (**Figure 2(a)**), with lower temperature and smaller evaporation, is the season with the least amount of PWV. The maximum PWV appears in South China Coast, with a value of about 24 mm. The minimum PWV appears in the Tibetan Plateau, with a value of only 2 mm. A wet tongue extends from the South China to the Sichuan Basin and a dry tongue extends from the eastern Tibetan Plateau to the Yunnan-Guizhou Plateau, which are related to the role of the Hengduan Mountain and the Sichuan Basin (Liao et al., 2013). It can be seen that the PWV contours in eastern China are the most consistent with the parallel, with the largest gradient and relatively uniform spacing, which are mainly affected by the geographic latitude and altitude. Affected by the East Asian summer monsoon, the PWV values increases significantly over Chinese mainland in summer (**Figure 2(c)**). The PWV in the South China Coastal can reach 54 mm and the PWV in the Tibetan Plateau can reach 10 mm. The range of dry tongue and wet tongue become larger and the PWV contours are

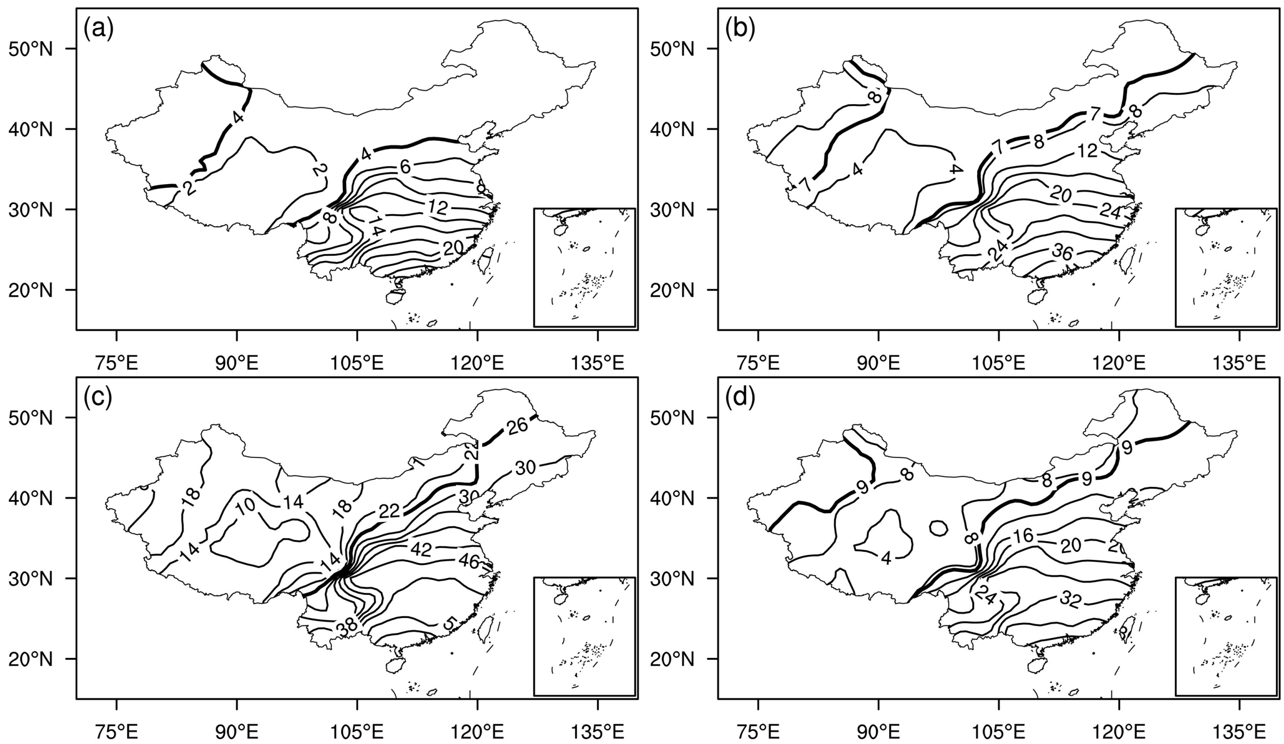

Figure 2. Seasonal averaged PWV over Chinese mainland in (a) winter, (b) spring, (c) summer and (d) autumn (unit: mm).

denser. It is worth noting that the PWV in Sichuan Basin is only smaller than that in the South China coast in summer, with a value of about 46 mm, which shows that the topography plays an essential role. At this time, the PWV contours in eastern China forms a large northeast-southwest angle with the parallel. The 26 mm PWV contour corresponds to the boundary between the monsoon region and the non-monsoon region in summer (**Figure 2(c)**). The PWV in the monsoon areas (southeast of the boundary) is significantly higher than that in the non-monsoon areas (northwest of the boundary), which shows that the East Asian summer monsoon has a major impact on the spatial distribution of PWV in summer. It is the medium in spring and autumn, with more in autumn than in spring (**Figure 2(b)**, **Figure 2(d)**). And there are similar spatial distributions of PWV in spring and autumn. The PWV contours in the south of 35˚N in eastern China are mainly unanimous with the parallel. While, the PWV contours in the north of 35˚N form a northeast-southwest obliquity, which are more parallel than that in summer.

3.2. Spatial Distribution of Annual and Seasonal Mean PWV Variation Coefficient over Chinese Mainland

To further analyze the variation amplitude of PWV, **Figure 3** shows the variation coefficient distribution of the annual averaged PWV in China from 1979 to 2014. In general, the variation coefficient of PWV is characterized by increasing from southeast China to northwest China, which is contrary to the spatial distribution of PWV (**Figure 1**). That is to say, the variation coefficient of PWV is

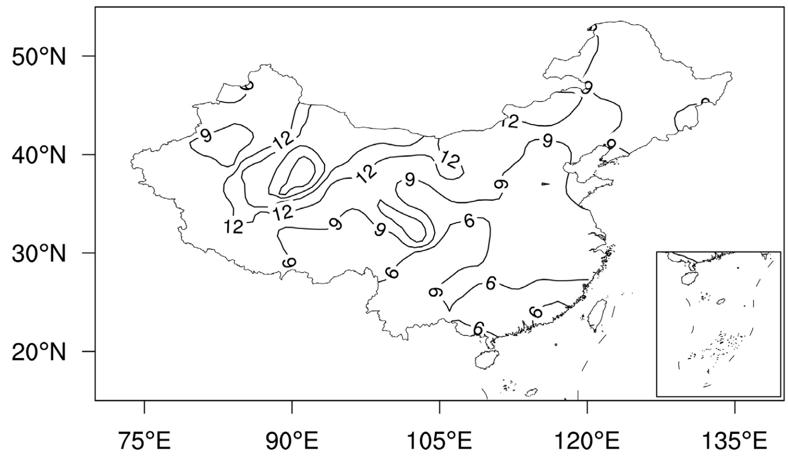

Figure 3. Annual mean PWV variance coefficient over Chinese mainland (unit: %).

smaller (larger) and the variation amplitude of is smaller (larger) in the areas with more (less) PWV. The 0.09 mm contour roughly corresponds to the boundary between the monsoon regions and the non-monsoon regions in China (**Figure 3**). Taking this line as the boundary, the variation coefficient of PWV in the monsoon areas with more PWV is obviously smaller than that in the non-monsoon area with less PWV. The regions with the smallest PWV variation coefficient are located in the Sichuan Basin and the south of Yunnan. The region with the largest PWV variation coefficient is located at the junction of Xinjiang and Qinghai.

Figure 4 further shows the variation coefficient of four seasonal PWV. Overall, the variation coefficient of seasonal mean PWV is characterized by increasing from southeast China to northwest China, which is also opposite to the spatial distribution of four seasonal PWV (**Figure 2**). Moreover, the variation coefficient of PWV has obvious seasonal difference. In winter (**Figure 4(a)**), PWV variation coefficient is the largest. The area with the smallest variation amplitude is located in Sichuan Basin and the areas with the largest variation amplitude are located at the junction of Xinjiang and Qinghai and the southwest of Xizang. In summer, the variation coefficient of PWV decreases markedly (**Figure 4(c)**). Taking the 0.08 contour as the boundary, the variation coefficient in the monsoon regions is smaller than that in the non-monsoon regions. The region with the smallest variation amplitude is located in South China and the region with the largest variation amplitude is located at the junction of Xinjiang and Qinghai. It is the medium in spring and autumn and their spatial distribution is roughly similar (**Figure 4(b)**, **Figure 4(d)**). The regions with the largest variation amplitude are located at the junction of Xinjiang and Qinghai. The region with the smallest variation amplitude is located in the Southeast China coast.

4. Temporal Evolution Characteristics of PWV

4.1. EOF Analysis

It can be seen that there are obvious regional and seasonal differences in the

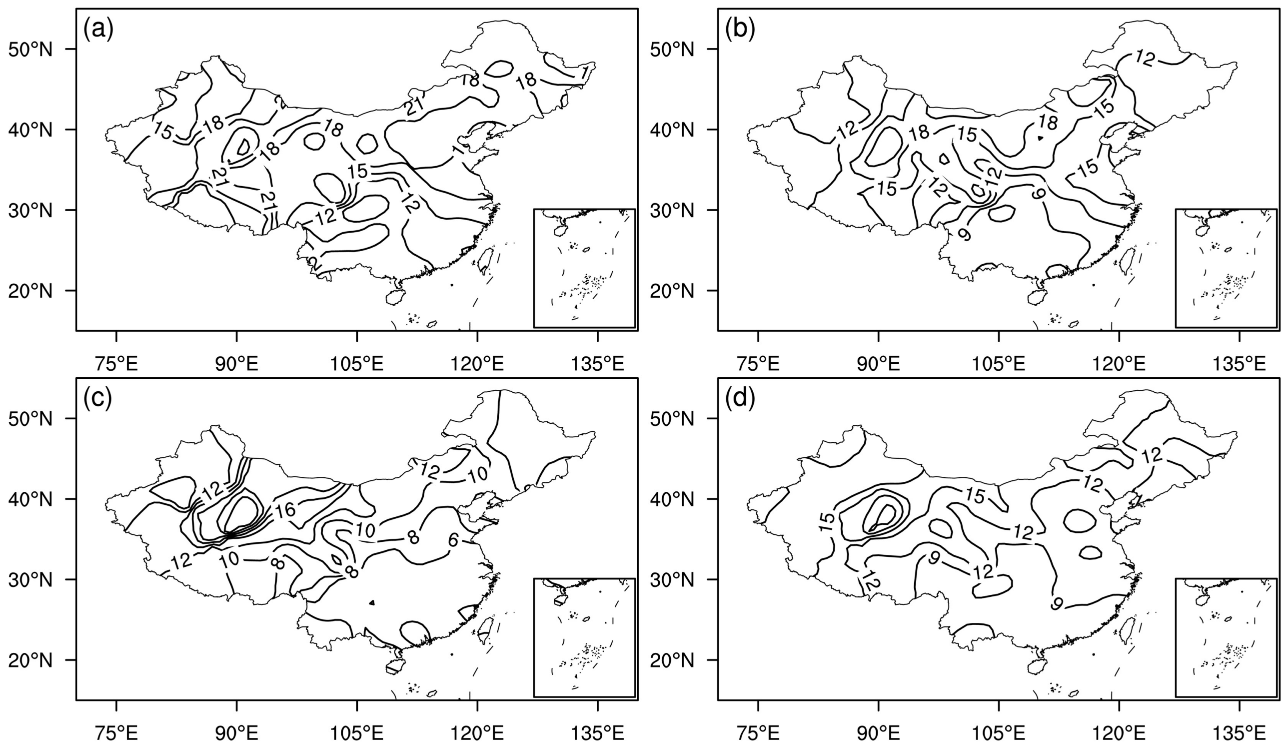

Figure 4. The variance coefficient of seasonal averaged PWV over Chinese mainland in (a) winter, (b) spring, (c) summer and (d) autumn (unit: %).

spatial distribution and variation amplitude of PWV over Chinese mainland according to the above analysis. Therefore, the EOF decomposition of the four seasonal PWV anomaly in China is further applied to examine the spatial distribution characteristics of the leading modes. Table 1 shows the variance contributions and cumulative variance contributions of the two leading EOFs of four seasonal PWV anomaly. The results show that the cumulative variance contributions of the two leading EOFs can reach 59%, which can represent the main distribution characteristics of PWV. Overall, the levels of the first mode variance contribution are highest in winter, followed by spring and autumn, and are lowest in summer.

Figure 5 shows the spatial distribution of the first EOF of four seasonal PWV anomaly. It shows that a consistent distribution pattern in the whole region and there are still obvious seasonal differences. In winter (Figure 5(a)), the variance contribution of the first mode is 74.2%, which has better convergence in spatial distribution. The large value area is located in the Southeast China coastal. In spring (Figure 5(b)), the large value area is located in eastern China. In summer (Figure 5(c)), the distribution of high PWV value centers is scattered and the convergence rate is the slowest, with a value of 48.8%, which reflect the complexity and variability of the spatial distribution of PWV. The spatial distribution pattern in autumn (Figure 5(d)) is similar to that in winter. In summary, it indicates that the first EOF shows a consistent distribution pattern in the whole region, which is roughly similar to the first EOF of Zhao et al. (2012). The

Table 1. Variance contributions and cumulative variance contributions (unit: %) of four seasonal PWV anomaly from EOF decomposition.

season	winter		spring		summer		autumn	
eigenvector	1	2	1	2	1	2	1	2
variance contributions	74.2	6.4	71.5	6.6	48.8	11.0	57.2	9.5
cumulative variance contributions	74.2	80.6	71.5	78.1	48.8	59.8	57.2	66.7

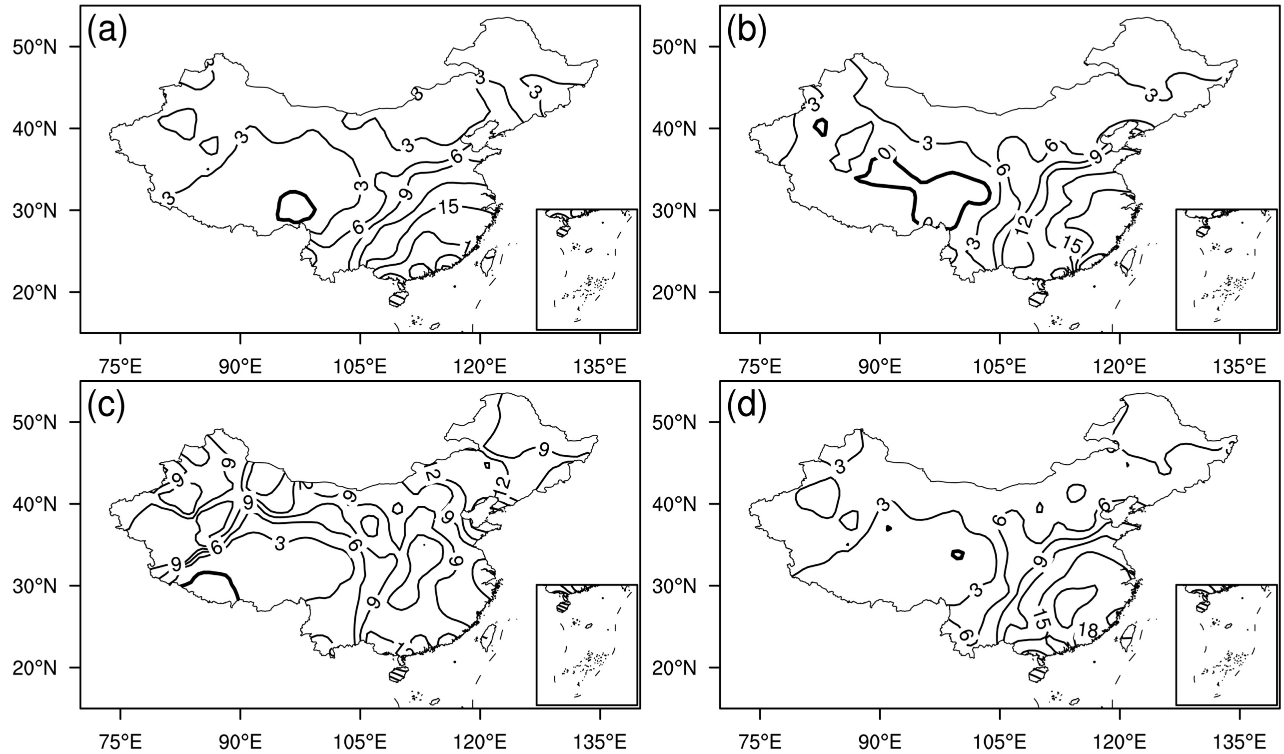

Figure 5. Spatial distribution of the first EOF of PWV anomaly in (a) winter, (b) spring, (c) summer and (d) autumn respectively; values have been multiplied by 100.

second EOF shows a dipole pattern between South and North China (not shown).

Figure 6 displays that the corresponding time coefficients of first EOF with the largest variance contribution to analyze the time variation characteristics of four seasonal PWV in China. The abnormal variation of four seasonal PWV shows obvious interdecadal oscillation. In winter, spring and summer (**Figures 6(a)-(c)**), it shows a consistent increasing trend before 2002, although there were interannual changes. However, it shows a consistent decreasing trend after 2002, which may result from the inhomogeneity of humidity data caused by the renewal of radiosonde instrument and the upgrading of detection system in China around 2002 (Dai et al., 2011; Zhao et al., 2012; Chen et al., 2015). In autumn (**Figure 6(c)**), PWV has an increasing-decreasing-increasing-decreasing trend, which shows higher-than-normal PWV anomalies during 1981-1990 and

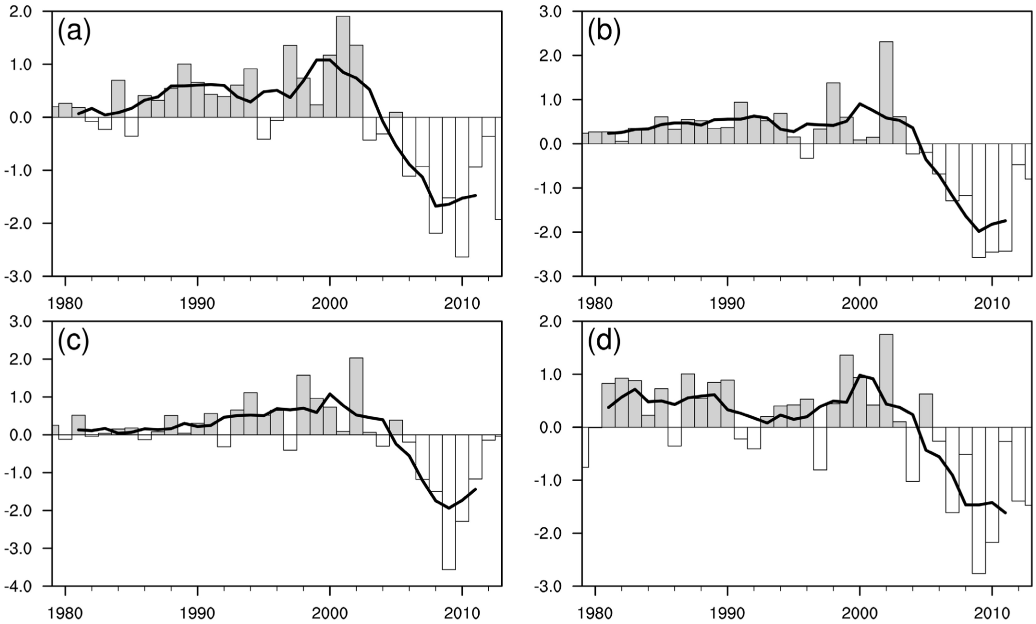

Figure 6. Time coefficients of the first EOF of PWV anomaly from in (a) winter, (b) spring, (c) summer and (d) autumn respectively; the black lines indicate 5 year running means.

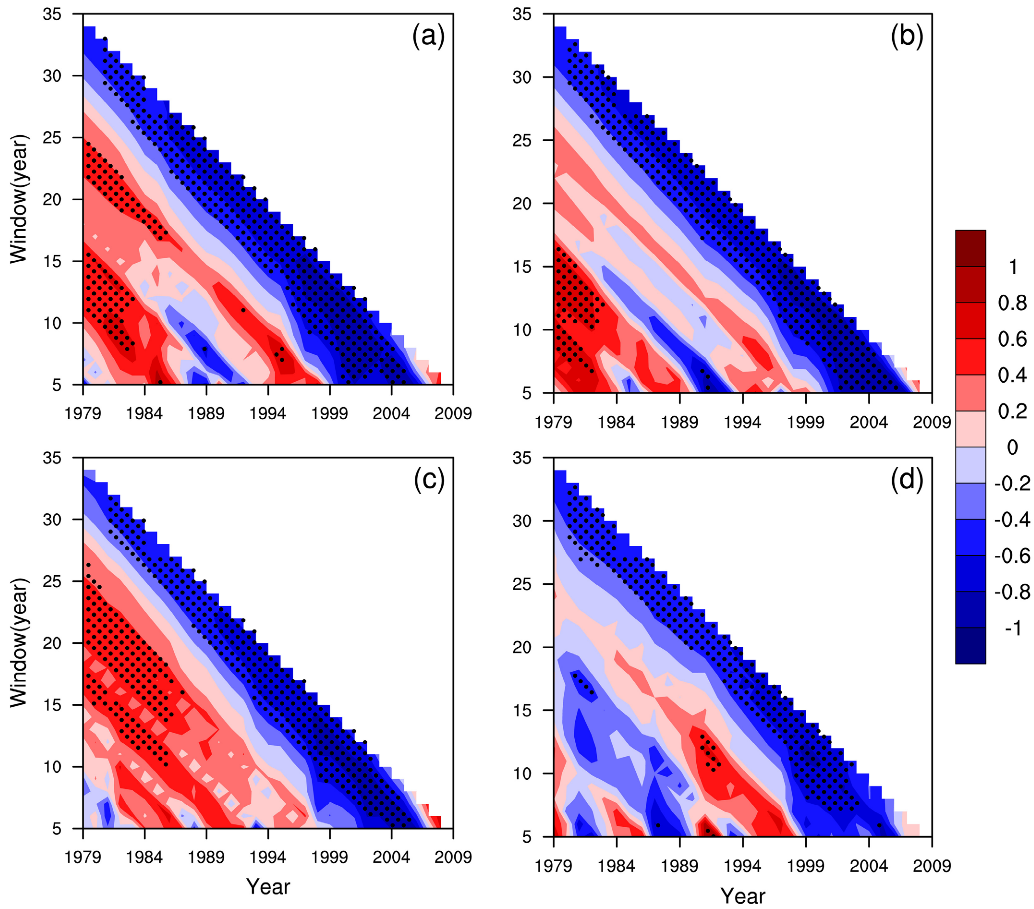

Figure 7. The running trend coefficients of PWV in (a) winter, (b) spring, (c) summer and (d) autumn respectively; the black dots are statistically significant at the 90% level.

1994-2002 and lower-than-normal PWV anomalies in other years.

4.2. Trend Analysis

In order to further analyze the long-term trend of four seasonal PWV, **Figure 7** presents the distribution of the sliding trend coefficient. The trend coefficient is calculated from 1979 until the end of the recording, with the increment of 1 year and the shortest sliding window of 5 years (Guo et al., 2017). It shows a consistent decreasing trend since 2002, although the trend coefficient of four seasonal PWV fluctuates. The decrease trend in winter is statistically significant at the 90% level. The trend in winter (**Figure 7(a)**) resembles the variation in spring (**Figure 7(b)**). The time window above 15 years shows an increasing trend, and the time window below 15 years has obvious fluctuations, showing the trend of increasing-decreasing-increasing-decreasing. In summer (**Figure 7(c)**), the PWV shows a robust growth trend, which is statistically significant at the 90% level in the time window of more than 10 years. In contrast, the time window below 10 years shows a weak growth trend. In autumn (**Figure 7(d)**), the fluctuations are more obvious and the overall trend is increasing—decreasing—increasing—decreasing.

5. Conclusion and Discussion

5.1. Conclusion

This paper calculates the annual and seasonal averaged PWV and further reveals the spatial distribution and temporal evolution characteristics of four seasonal PWV over Chinese mainland, based on the observed temperature and humidity data of 102 radiosonde stations from 1979 to 2014.

The spatial distribution of annual mean and seasonal mean PWV in China shows obvious geographical differences, which are generally characterized by low-latitude regions greater than high-latitude regions, plain regions greater than plateau regions, coastal regions greater than inland regions, and decreasing from southeast to northwest. The levels of PWV are lowest in winter, followed by spring and autumn, and are highest in summer. The PWV contours in winter over eastern China are the most consistent with the parallel, with the largest gradient and relatively uniform spacing, which are mainly affected by geographic latitude and altitude. The PWV contours in summer over eastern China form a large northeast-southwest angle with the parallel, which is mainly affected by the East Asian summer monsoon.

The spatial distribution pattern of four seasonal PWV is approximately opposite to the distribution pattern of the variation coefficient, that is, the monsoon region with more PWV has a smaller variation coefficient and smaller variation amplitude, while the non-monsoon area with less PWV has a larger variation coefficient and has larger variation amplitude. Besides, there are obvious seasonal differences and extreme value centers differences.

The cumulative variance contributions of the first two modes of four seasonal

PWV from EOF decomposition can reach 51%, which can represent the main distribution characteristics of PWV. The first EOF has a consistent distribution pattern in the whole region and the feature is most significant in winter. The abnormal variation of four seasonal PWV shows obvious interdecadal oscillation. Meanwhile, it shows an apparent decreasing trend after 2002, which may be due to the renewal of radiosonde instruments in China around 2002.

5.2. Discussion

Although the paper has obtained some meaningful conclusions, there are still some shortcomings that need further research. Due to the scarcity of radiosonde stations and the coarse spatial resolution in western China (**Figure 1**), the results in western China need to be discussed. With the development of satellite remote sensing technology (Gao & Kaufman, 2003; Chen & Liu, 2016; Nelson et al., 2016; Chen et al., 2018; Jiang et al., 2019), it can contribute to the study of water vapor in these regions. The inhomogeneity of humidity data caused by the renewal of radiosonde instruments and the upgrading of detection system in China after 2002 will lead to false trend variation. Therefore, more analyses about trend evolution of PWV before and after the upgrading of the radiosonde stations will be conducted in the future.

Acknowledgements

This research was jointly supported by the National High Technology Research and Development Program of China (Grant No. 2018YFC1505705), State Key Program of National Natural Science Foundation of China (Grant Nos. 42030602; 42030611).

Conflicts of Interest

The authors declare no conflicts of interest regarding the publication of this paper.

References

Brettle, M. J., & Galvin, J. F. P. (2003). Back to Basics: Radiosondes: Part 1—The Instrument. *Weather, 58,* 336-341. https://doi.org/10.1256/wea.126.02A

Chahine, M. T. (1992). The Hydrological Cycle and Its Influence on Climate. *Nature, 359,* 373-380. https://doi.org/10.1038/359373a0

Chen, B. Y., & Liu, Z. Z. (2016). Global Water Vapor Variability and Trend from the Latest 36 Year (1979 to 2014) Data of ECMWF and NCEP Reanalyses, Radiosonde, GPS, and Microwave Satellite. *Journal of Geophysical Research: Atmospheres, 121,* 11442-11462. https://doi.org/10.1002/2016JD024917

Chen, B. Y., Dai, W. J., Liu, Z. Z. et al. (2018). Assessments of GMI-Derived Precipitable Water Vapor Products over the South and East China Seas Using Radiosonde and GNSS. *Advances in Meteorology, 2018,* Article ID: 7161328. https://doi.org/10.1155/2018/7161328

Chen, Z., Yang, S., & Liu, L. K. (2015). Inhomogeneity Test and Correction of China Radiosondes Relative Humidity Data from 1979 to 2012. *Meteorological Monthly, 41,* 1374-1382.

Dai, A. G., Wang, J. H., Thorne, P. W. et al. (2011). A New Approach to Homogenize Daily Radiosonde Humidity Data. *Journal of Climate, 24,* 965-991. https://doi.org/10.1175/2010JCLI3816.1

Dai, Y., & Yang, X. Q. (2009). Spatial-Temporal Variations of Precipitable Water over China. *Scientia Meteorologica Sinica, 29,* 143-149.

Fontaine, B., Roucou, P., & Trzaska, S. (2003). Atmospheric Water Cycle and Moisture Fluxes in the West African Monsoon: Mean Annual Cycles and Relationship Using NCEP/NCAR Reanalysis. *Geophysical Research Letters, 30,* Article No. 1117. https://doi.org/10.1029/2002GL015834

Gao, B. C., & Kaufman, Y. J. (2003). Water Vapor Retrievals Using Moderate Resolution Imaging Spectroradiometer (MODIS) Near-Infrared Channels. *Journal of Geophysical Research, 108,* Article No. 4389. https://doi.org/10.1029/2002JD003023

Guo, J. P., Su, T. N., Li, Z. Q. et al. (2017). Declining Frequency of Summertime Local-Scale Precipitation over Eastern China from 1970 to 2010 and Its Potential Link to Aerosols. *Geophysical Research Letters, 44,* 5700-5708. https://doi.org/10.1002/2017GL073533

Guo, J., & Li, G. P. (2009). Climatic Characteristics of Precipitable Water Vapor and Relations to Surface Water Vapor Column in Sichuan and Chongqing Region. *Journal of Natural Resources, 24,* 344-350.

Held, I. M., & Soden, B. J. (2000). Water Vapor Feedback and Global Warming. *Annual Review of Energy and the Environment, 25,* 441-475. https://doi.org/10.1146/annurev.energy.25.1.441

Huang, L., Fan, G. Z., Lai, X. et al. (2018a). Change Characteristics of Precipitation Water Vapor Qinghai-Tibetan Plateau during 1979-2015. *Journal of Southwest University (Natural Science Edition), 40,* 94-103.

Huang, X. Y., Wang, S. J., & Wang, X. P. (2018b). Variations of Precipitable Water in Northwest China during 1960-2015. *Meteorological Monthly, 44,* 1191-1199.

Jia, B. X., Xu, H. M., & An, Y. G. (2014). Comparisons of Atmospheric Specific Humidity in Reanalysis Datasets and Homogenized Radiosonde Dataset in China. *Meteorological Monthly, 40,* 1123-1131.

Jiang, J., Zhou, T. J., & Zhang, W. X. (2019). Evaluation of Satellite and Reanalysis Precipitable Water Vapor Data Sets against Radiosonde Observations in Central Asia. *Earth and Space Science, 6,* 1129-1148. https://doi.org/10.1029/2019EA000654

Kiehl, J. T., & Trenberth, K. E. (1997). Earth's Annual Global Mean Energy Budget. *Bulletin of the American Meteorological Society, 78,* 197-208. https://doi.org/10.1175/1520-0477(1997)078<0197:EAGMEB>2.0.CO;2

Liao, A. M., Liu, J. F., & Zhou, G. L. (2013). Trends in Moisture Content for 1979-2010 in China River Basins. *Advances in Water Science, 24,* 626-633.

Liu, D., Qiu, X. F., Shi, L. et al. (2013a). Estimation of Atmospheric Precipitable Water in China with NCEP Data and Its Spatio-Temporal Distribution. *Journal of Nanjing University of Information Science and Technology: Natural Science Edition, 5,* 113-119.

Liu, Z. Z., Wong, M. S., Nichol, J. et al. (2013b). A Multi-Sensor Study of Water Vapour from Radiosonde, MODIS and AERONET: A Case Study of Hong Kong. *International Journal of Climatology, 33,* 109-120. https://doi.org/10.1002/joc.3412

Lu, Y. R., & Gao, G. D. (1984). The Water Vapour Content and the Water Budget in the Atmosphere over China. *Acta Meteorologica Sinica, 42,* 301-310.

Ma, X. P., Shang, K. Z., Li, J. Y. et al. (2015). Spatial and Temporal Changes of Atmospheric Precipitable Water in the Eastern Part of Northwest China from 1981 to 2010. *Journal of Desert Research, 35,* 448-455.

Nelson, R. R., Crisp, D., Ott, L. E. et al. (2016). High-Accuracy Measurements of Total Column Water Vapor from the Orbiting Carbon Observatory-2. *Geophysical Research Letters, 43,* 12261-12269. https://doi.org/10.1002/2016GL071200

Oikonomou, E. K., & O'Neill, A. (2006). Evaluation of Ozone and Water Vapor Fields from the ECMWF Reanalysis ERA-40 during 1991-1999 in Comparison with UARS Satellite and MOZAIC Aircraft Observations. *Journal of Geophysical Research, 111,* D14109. https://doi.org/10.1029/2004JD005341

Shi, Y. G., & Sun, Z. B. (2008). Climate Characteristics of Atmospheric Precipitable Water over Xinjiang and Its Variation. *Journal of Desert Research, 28,* 519-525.

Trenberth, K. E., Fasullo, J., & Smith, L. (2005). Trends and Variability in Column-Integrated Atmospheric Water Vapor. *Climate Dynamics, 24,* 741-758. https://doi.org/10.1007/s00382-005-0017-4

Trenberth, K. E., Smith, L., Qian, T. et al. (2007). Estimates of the Global Water Budget and Its Annual Cycle Using Observational and Model Data. *Journal of Hydrometeorology, 8,* 758-769. https://doi.org/10.1175/JHM600.1

Wagner, T., Beirle, S., Grzegorski, M. et al. (2006). Global Trends (1996-2003) of Total Column Precipitable Water Observed by Global Ozone Monitoring Experiment (GOME) on ERS-2 and Their Relation to Near-Surface Temperature. *Journal of Geophysical Research: Atmospheres, 111,* D12102. https://doi.org/10.1029/2005JD006523

Wang, P., Xie, T. C., Dai, J. G. et al. (2017). Trends and Variability in Precipitable Water Vapor throughout North China from 1979 to 2015. *Advances in Meteorology, 2017,* Article ID: 7804823. https://doi.org/10.1155/2017/7804823

Wei, F. Y. (2007). *Diagnotic and Predictive Technology in Modern Climatologic Statistics* (2nd ed.). China Meteorological Press.

Wong, M. S., Jin, X. M., Liu, Z. Z. et al. (2015). Multi-Sensors Study of Precipitable Water Vapour over Mainland China. *International Journal of Climatology, 35,* 3146-3159. https://doi.org/10.1002/joc.4199

Xie, X., He, J. H., & Qi, L. (2011). A Review on Applicability Evaluation of Four Reanalysis Datasets in China. *Journal of Meteorology and Environment, 27,* 58-65.

Yang, Q., Yao, J. Q., Zhao, Y. et al. (2013). Spatial-Temporal Variation of Water Vapor and Its Relationship with the Precipitation in the Ili River Basin. *Journal of Desert Research, 33,* 1174-1183.

Zhai, P. M., & Eskridge, R. E. (1997). Atmospheric Water Vapor over China. *Journal of Climate, 10,* 2643-2652. https://doi.org/10.1175/1520-0442(1997)010<2643:AWVOC>2.0.CO;2

Zhao, T. B., Dai, A. G., & Wang, J. H. (2012). Trends in Tropospheric Humidity from 1970 to 2008 over China from a Homogenized Radiosonde Dataset. *Journal of Climate, 25,* 4549-4567. https://doi.org/10.1175/JCLI-D-11-00557.1

Zhao, T. B., Fu, C. B., Ke, Z. J. et al. (2010). Global Atmosphere Reanalysis Datasets: Current Status and Recent Advances. *Advances in Earth Science, 25,* 242-254.

Zheng, S. Z., & Yang, D. Q. (1962). Distribution of Precipitable Water over China. *Acta Geographica Sinica, 28,* 123-136.

Zhou, S. W., Wu, P., Wang, C. H. et al. (2011). Spatial Distribution of Atmospheric Water Vapor and Its Relationship with Precipitation in Summer over the Tibetan Plateau. *Acta Geographica Sinica, 66,* 1466-1478.

Zhu, Q. G., Lin, J. R., Shou, S. W. et al. (2000). *Principles and Applications of Synoptic*

Meteorology. China Meteorological Press.

Zou, J. S., & Liu, H. L. (1981). The Basic Features of Water Vapor Content and Their Controlling Factors in China. *Acta Geographica Sinica, 36,* 377-391.